Desalination 541 (2022) 116031

Contents lists available at ScienceDirect

Desalination

journal homepage: www.elsevier.com/locate/desal

Activated carbon as a photothermal absorber in PVDF membranes for solar driven air-gap membrane distillation

Maryam Alqaydi [a,b,1], Musthafa O. Mavukkandy [b,d,1], Ibrahim Mustafa [a,b], Aaesha Alnuaimi [c], Hassan A. Arafat [a,b,*], Faisal Almarzooqi [a,b,*]

[a] Department of Chemical Engineering, Khalifa University, PO Box 127788, Abu Dhabi, United Arab Emirates
[b] Center for Membranes & Advanced Water Technology (CMAT), Khalifa University, PO Box 127788, Abu Dhabi, United Arab Emirates
[c] Dubai Electricity and Water Authority (DEWA) Innovation Centre, Dubai Electricity & Water Authority, Dubai, United Arab Emirates
[d] Department of Environmental and Public Health, College of Health Sciences, Abu Dhabi University, PO Box 59911, Abu Dhabi, United Arab Emirates

HIGHLIGHTS

- A solar driven air gap membrane distillation unit was developed for desalination.
- Activated carbon (AC) was used as a solar absorbing material in the membranes.
- Even at low concentrations, AC boosted the solar-energy-driven flux of AGMD.
- Blending of 5 to 9 %AC into the PVDF matrix boosted the flux by 281–1400 %.
- PVDF-9%AC exhibited a normalized MD coefficient value of 18.8E-5 kg s^{-1} m^{-3} Pa^{-1}.

ARTICLE INFO

Keywords:
Membrane distillation
Solar desalination
Photothermal membrane
Activated carbon
Temperature polarization

ABSTRACT

Renewable energy-enabled desalination systems are crucial for solving the global water scarcity challenges in an environmentally friendly manner. In this work, we report an air gap membrane distillation (AGMD) process that utilizes polyvinylidene fluoride (PVDF) membranes blended with a photothermally active and relatively inexpensive activated carbon (AC). The composite membrane absorbed the solar radiation and generated local heat at the membrane surface, providing the driving force required in the AGMD process. This strategy overcame one of the key limitations of traditional MD—temperature polarization, and increased the energy efficiency significantly. We show that the blending of 5 to 9 %AC into the PVDF matrix can significantly boost the solar-energy-driven flux of AGMD by 281–1400 %, compared to the pristine membrane. PVDF membrane blended with 9 %AC exhibited an average AGMD permeate flux of 0.31 $kg.m^{-2}.h^{-1}$, with a GOR of 0.29 and a photothermal efficiency of 17.64 %. All PVDF-AC membranes showed excellent salt rejection, reaching 99.9 % for PVDF-9%AC. Finally, the AGMD performance of the fabricated membranes was compared by estimating their normalized MD coefficients (B/δ). PVDF-9%AC exhibited a B/δ value of 18.8E-5 kg s^{-1} m^{-3} Pa^{-1}, as opposed to a meager 0.89E-5 kg s^{-1} m^{-3} Pa^{-1} exhibited by its pristine counterpart.

1. Introduction

Water scarcity affects 3.7 billion people worldwide, which could rise to 5.7 billion by 2050 [1]. Therefore, the rate of desalinated water production was projected to grow at an annual rate of 9 % between 2018 and 2022 [2], highlighting the need for further research in this field. Desalination plants, traditionally powered by fossil fuels, face a key challenge as they consume high amounts of fossil energy and have high associated costs [3]. Their harmful environmental effects call for more dependency on renewable energy sources [4,5].

Membrane distillation (MD) is an emerging desalination technology where the temperature differential between the hot feed solution and cold permeate side drives the desalination process. Water from the liquid feed is moved in its vapor phase through a hydrophobic

* Corresponding authors at: Department of Chemical Engineering, Khalifa University, PO Box 127788, Abu Dhabi, United Arab Emirates.
E-mail addresses: hassan.arafat@ku.ac.ae (H.A. Arafat), faisal.almarzooqi@ku.ac.ae (F. Almarzooqi).
[1] These authors contributed equally to this work.

https://doi.org/10.1016/j.desal.2022.116031
Received 20 March 2022; Received in revised form 23 July 2022; Accepted 3 August 2022
Available online 9 August 2022

microporous membrane, generating a permeate that has negligible amounts of salts. MD provides various benefits over conventional desalination processes, including minimal electrical energy requirements, flexibility to run on low-grade heat, lower membrane fouling tendency, and the capacity to handle difficult-to-treat hypersaline feed water. In air gap MD (AGMD), a popular MD configuration, an air gap is placed on the cold side such that the permeate condenses on a chilled plate after travelling through the air gap. The main advantage of this configuration is that the thermally insulating air gap could maintain the temperature gradient across the membrane [6].

There have been several attempts to couple solar energy with MD—either by producing the thermal energy for driving the evaporation/distillation or by generating electricity for enabling the MD process [7]. However, conventional solar MD equipped with external solar thermal collectors have several disadvantages, such as higher heat loss, temperature polarization, and low energy efficiency. On the other hand, photothermal-assisted MD, which involves localized membrane heating by direct absorption of sunlight energy at the membrane surface, could overcome several of these limitations. Summers and Lienhard studied such a photothermal AGMD concept and reported a permeate flux ~0.35 $kg.m^{-2}.h^{-1}$ [8]. The energy efficiency of their system was improved by distributing heat to the membrane surface, where the incident solar radiation evaporates the water. Recent progress in photothermal materials has yielded many promising candidates as solar absorbers.

Recent progress in solar absorbers has revealed numerous photothermal materials, such as semiconductor particles as well as polymeric, carbonaceous and plasmonic materials. To be practical, these materials should possess strong absorption in the broad solar spectrum, be stable even at high temperatures, and be inexpensive [9]. For instance, in a previous study, photothermal carbon black (CB) was suspended in polyvinyl alcohol (PVA) solution and electrospun on a polydopamine-coated polyvinylidene fluoride (PVDF) support membrane to obtain a network of photo-absorbing CB-laden PVA nanofibers on PVDF membrane [10]. When tested in direct contact MD (DCMD) configuration under focused solar irradiation, a flux of ~5.38 $kg.m^{-2}.h^{-1}$ was obtained with a salt rejection exceeding 99.5 % and a solar efficiency higher than 20 %. In another study, Huang et al. demonstrated the reduction in temperature polarization in vacuum MD by incorporating antimony doped tin oxide as a photothermal material in PVDF nanofiber membranes, which increased the MD flux from 8.0 to 27.0 $kg.m^{-2}.h^{-1}$, under infrared radiation [11]. In another study, membranes incorporated with carbon black or SiO_2/Au nanoshells exhibited ~33.0 % higher flux in DCMD when exposed to simulated solar radiation of 1 sun, without compromising salt rejection [12]. Others used Fe_3O_4/PVDF-HFP nanofibrous membrane [13], PVDF/Ag hybrid membranes [14], polydopamine-coated PVDF membrane [15], and PVDF membrane incorporated with titanium nitride nanoparticle [16] to induce photothermal capabilities in MD membranes, decrease the temperature polarization, and improve the permeate flux. Thus, most previous photothermal MD studies have been utilizing relatively high-cost materials (e.g. plasmonic materials) due to their enhanced photothermal properties. However, considering the material cost is also essential to improve the practical feasibility of such innovative systems; hence we demonstrate the application of a relatively low-cost material (i.e., activated carbon) as a candidate for such photothermal AGMD applications. Zhao et al. blended different concentrations (0–3 wt%) of activated carbon (AC) nanoparticles into PVDF-HFP electrospun membranes to produce hydrophobic/hydrophilic bilayer nanofiber membrane and tested them in DCMD for enhanced flux [17]. However, the photothermal capabilities of AC particles were not investigated in that study.

In a recent work, our group tested phase-inverted PVDF membranes blended with high concentrations of AC (up to 50 %) in an AGMD for removing heavy metals (Zn^{2+}, Ni^{2+}, Cr^{3+}, Fe^{3+}, and Cu^{2+}) from wastewater and found that PVDF-AC membranes could efficiently reject heavy metal ions [18]. Although these phase-inverted PVDF membranes have several advantages, such as good interlinking of the AC with the PVDF matrix, thereby minimizing the leaching, the use of high additive loading can cause issues with membranes integrity and stability, especially when the process involves direct solar irradiation to heat up the membrane. Hence, membranes created with lower additive concentrations without compromising the photothermal performance, could be advantageous in this case. Thus, in this work, we fabricated phase inverted PVDF-AC membranes with significantly lower AC concentrations (only up to 9 %) than in our previous study [18] and demonstrated their application in solar-assisted AGMD for desalination application. We show that even at relatively low concentrations, AC can significantly boost the solar-energy-driven flux of AGMD and achieve low energy demand and high energy efficiency, when compared to similar black body materials in solar-assisted AGMD applications.

2. Methodology

2.1. Material

Dimethylacetamide (DMAc, >99.5 %, Sigma Aldrich) was used to dissolve polyvinylidene fluoride (PVDF-741, Kynar HSV900). Activated carbon (AC, Sigma Aldrich with a particle size ranging from 8.65 to 47.65 μm) was used as a hydrophilic blackbody additive. A non-woven porous material (Novatexx 2471, Freudenberg-Filter, Germany) was used as a hydrophobic inlay between the cast membrane and the air gap. Deionized water (DI, Purity, ×18.2 MΩcm) was utilized in all experiments.

2.2. Photothermal membrane fabrication

Non-solvent induced phase separation was employed to fabricate the photothermal AC-blended membranes, as shown in Fig. 1. First, 12 g of PVDF polymer were added to a beaker containing a pre-determined mass of DMAc (as shown in Table 1) and mixed at 200 rpm for 24 h followed by bath sonication for 30 min to get rid of trapped air bubbles. The dope solution was then allowed to rest and degas for 2 h. At that stage, a pre-determined mass of activated carbon (Table 1) was added to the solution and the mixing, sonication, and resting steps were repeated. Then, the dope solution was cast onto a non-woven porous support (Novatexx 2471) using a casting knife (MTI, EQ-Se-KTQ-100, USA). The wet membrane thickness was set at 500 μm. The phase separation was then triggered by dipping the cast film in a DI water coagulation bath, after which the nascent membrane was air-dried for 24 h on a laminar airflow workstation (NU-340, Airegard, USA) at a regulated airflow of 0.46 ms^{-1}.

2.3. Membrane characterization

Scanning electron microscopy (SEM, Nova 600 NanoLab, Netherlands) was used to study the morphology of the membranes. The membrane coupons were coated with Au/Pd thin films (10 nm thickness) before acquiring the images using a precision coater (Gatan Inc., PECS 862, USA) to avoid the polymeric charging effects. Working distance was fixed at 10 mm, and SEM images were obtained under vacuum. Light absorbance of the blend membranes over the wavelength of 250 to 2500 nm was obtained using a spectrometer (LAMBDA 1050+ UV/Vis/NIR, Perkin-Elmer Germany). Membrane wettability was analyzed using a goniometer (DSA 10Mk2, Krüss, Germany) at room temperature, and contact angles were obtained from the droplet images, as detailed elsewhere [19]. Thermal conductivity was measured using a flash diffusivity device (TPS2500 S, Hot Disc, Sweden) [18]. Porosity was determined gravimetrically. The weight of a dry membrane coupon was determined and then wetted with a liquid with known surface tension (Galwick®, obtained from PMI Inc., USA). The weight of the wet membrane was re-recorded. The volume porosity was then calculated from the wet and dry mass differences. Membrane pore sizes were

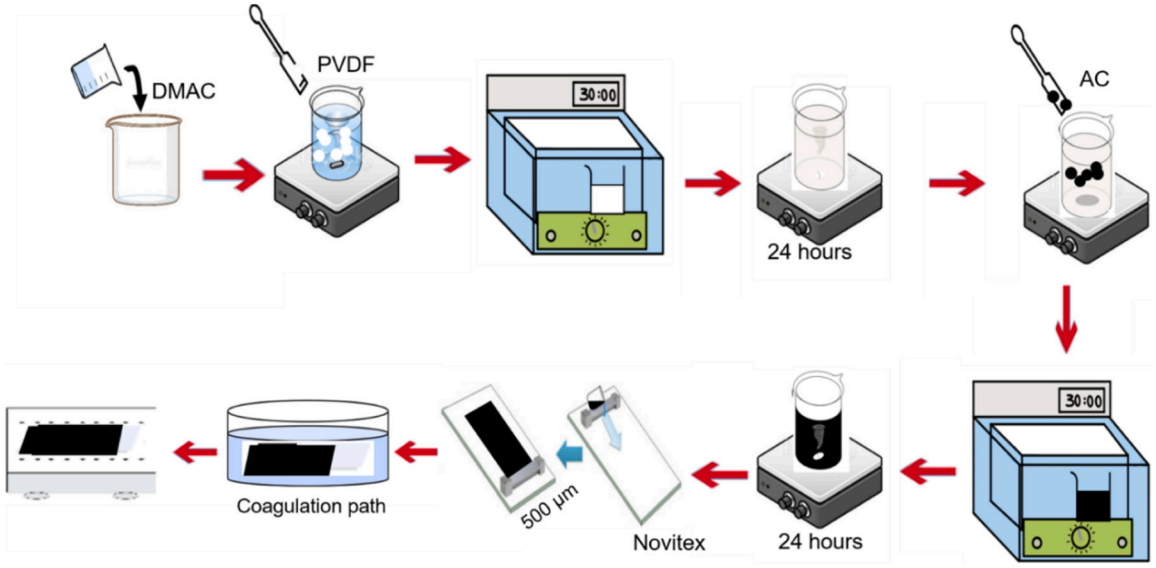

Fig. 1. Fabrication steps of phase inverted PVDF-AC membranes.

Table 1
Mass compositions of the polymer dope solutions employed in the study.

Membrane	Mass of PVDF (g)	Mass of AC (g)	Mass of DMAc (g)
PVDF	12	0	88
PVDF-AC5%	12	5	83
PVDF-AC7%	12	7	81
PVDF-AC9%	12	9	79

determined via capillary flow porometry (CFP, PMI Inc., USA), by pre-wetting the membranes with Galwick (PMI Inc., USA) and pushing the liquid inside the pores by applying incremental pressure (more details can be found in [20,21]).

2.4. AC leaching from the PVDF membrane

The AC nanoparticles' stability within the membrane matrix was evaluated gravimetrically according to the previously reported procedure [22,23]. Initially, a sample coupon of AC-blended membranes (2 × 1 cm^2) was kept in a vacuum oven (60 °C, 100 mbar) for 24 h, and the dry sample weight was determined. The dried sample was then dipped in a glass beaker with DI water (100 mL) and shaken for 24 h at 800 rpm. Finally, the membrane was lifted, re-dried in the vacuum oven (60 °C, 100 mbar), and its dry weight was measured again. The leaching of AC nanoparticles was assessed by determining the difference between initial and final weights.

2.5. Photothermal AGMD tests

The photothermal AGMD performance of the membranes was tested in a custom-built AGMD setup, as illustrated in Fig. 2. The experimental setup comprised a tailor-made acrylic module cell, a feedwater loop, a cooling water loop, and a solar simulator. The feed solution (35 g/L NaCl in DI water) was pumped into the acrylic module using a peristaltic pump and was returned to the saline water reservoir via the feed outlet. A fixed volume (2 L) of cooling water was cooled down to 10 °C using a chiller and continuously circulated behind the condensation plate of the AGMD cell. As permeate water was generated during this process, the condensed permeate dripped into a collection container, and its weight was recorded continuously using an electronic balance. Since the PVDF-AC membrane was hydrophilic and readily wetted upon contact with feed in AGMD, a commercial hydrophobic PVDF membrane (PVDF Transfer Membrane, Thermo Scientific™, mean pore size of 0.2 μm, average contact angle of 109.2) was used as an interlay between the PVDF-AC membrane and the air gap, thus preventing the contamination of permeate with saline feed. This commercial membrane, thanks to its relatively lower thermal conductivity compared to the PVDF-AC membranes, also reduced the heat loss from the feed side. At pre-set intervals, the inlet and outlet feed temperature and permeate mass were recorded. A solar simulator (Newport Corp., 94082A, USA) equipped with a xenon lamp (UXL-16SB, Ushio, XE1600 W) provided the solar heat to be absorbed by the membrane, which drove the MD process. The solar irradiation power was set to 1.0 kW/m^2. A 24-hour experiment was carried out at room temperature (23 °C) for each test. The salt rejection and flux were determined based on the obtained permeate water characteristics.

The following equation depicts the water vapor transport across the membrane [24]:

$$J = B(P_H - P_C)$$

where J is the permeate flux, B stands for the MD coefficient (i.e., mass transfer coefficient), P_H is the vapor pressure of the hot water (feed water), and P_C is the vapor pressure on the permeate side. The vapor pressure can be estimated by using Antoine equation [25]. The theoretical maximum flux was obtained by dividing the solar energy incident on the membrane by the heat of evaporation of the feed water. Based on a solar irradiation power of 1.0 kW/m^2 and a heat of evaporation of 2.36 × 10^6 J/kg, the maximum theoretical flux was calculated as 1.48 kg. $m^{-2}.h^{-1}$. The photothermal efficiency of the MD system was calculated as:

$$\eta = \frac{Actual\ flux}{Max\ theortical\ flux}$$

The gained output ratio (GOR) is a measure of thermal efficiency of a desalination system and can be defined as follows for MD [8]:

$$GOR = \frac{J_m \times h_{fg}}{I}$$

where J_m is permeate flux, I is the thermal energy input to the MD system (assumed to be the incident solar radiation in this case) [W/m^2], and h_{fg} is the latent heat of feed evaporation [J/kg].

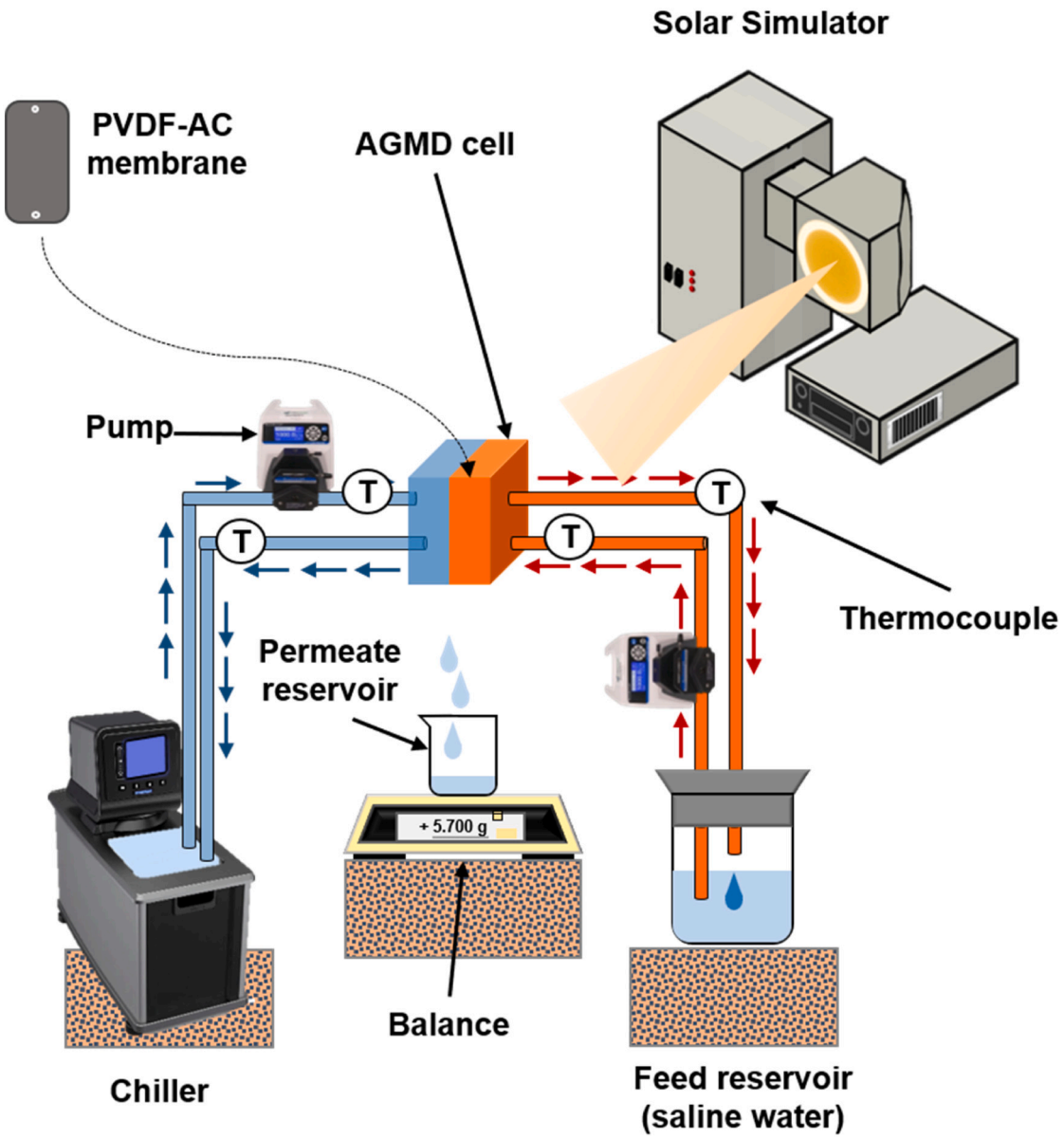

Fig. 2. Illustration of the custom-built AGMD device assisted by solar irradiation (inspired from our previous work [18]).

3. Results and discussion

3.1. Optical and structural characteristics of PVDF-AC membranes

The solar absorption properties and structural morphology of the photothermal membrane are crucial to its AGMD performance. SEM images were analyzed to examine the surface morphology of the pristine and AC-blended membranes. Fig. 3, showing top layer SEM micrographs at 3 magnifications, indicate that all membranes have a characteristic microporous topology. At lower magnifications, the dark spots distinctive to membranes made by NIPS process were visible, which resulted from some pore agglomeration. During the NIPS process, the cast films were immersed in the water bath, which initiated rapid demixing. A detailed examination of top layer micrographs reveals that as the concentration of AC in the polymer solution increased, it caused some aggregation on the surface (Fig. 3). Higher loading of AC particles can trigger the rapid migration of a few AC particles to the top surface to minimize the interface energy, as reported elsewhere [26,27].

Membrane thickness values are shown in Table 2. The solvent evaporates from the cast film during phase separation, lowering the thickness of the formed membranes and resulting in a deviation from the initially set casting thickness. Also, the thickness of the membranes increased with AC concentration which can be attributed to the formation of macro-voids and the development of finger-like substructures into wider and thicker forms as a result of the rapid demixing of dope solution, as reported elsewhere [28,29]. These results suggest that AC fillers played a role in defining the microstructure of the resultant microporous membrane.

Table 2 demonstrates a rise in thermal conductivity of membranes proportional to AC concentration in the composite membrane. The amount of conductive moieties in the polymer membrane matrix increases as the AC content increases, thus enhancing the thermal conductivity of the AC-blended membranes. A similar trend was reported elsewhere [30].

The wettability of the pristine and AC-blended PVDF membranes is also an essential feature for MD. It was herein determined by measuring the membranes' water CA. As presented in Fig. 4, AC-blended membranes had a higher hydrophilicity than the pristine PVDF membrane, due to several oxygenated moieties at the edges of AC, formed upon the oxidation of carbon [31]. The PVDF-3%AC was at the borderline of

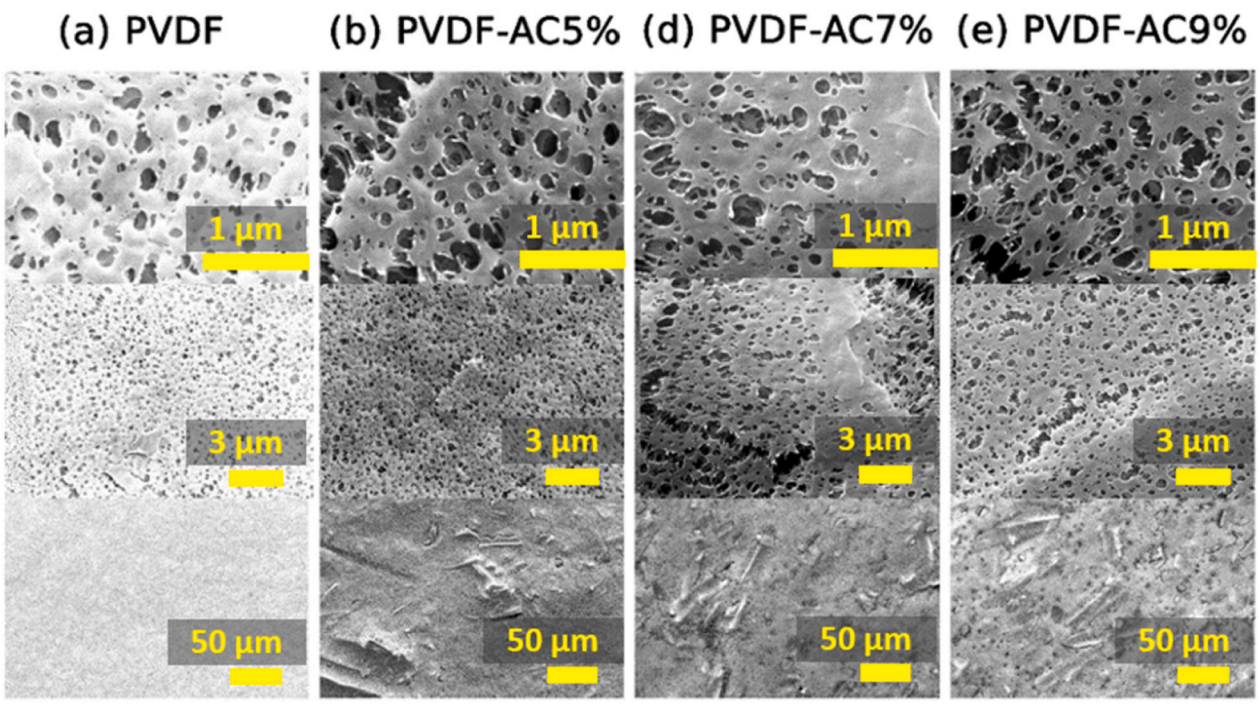

Fig. 3. SEM images probed for our PVDF-AC membranes.

Table 2
Physical characteristics of the membranes tested in the study.

Membrane	Thickness (mm)	Thermal conductivity (W/mK)
Commercial PVDF	0.16 ± 0.02	0.38 ± 0.09
PVDF	0.23 ± 0.02	0.24 ± 0.02
PVDF-5%AC	0.34 ± 0.02	2.23 ± 0.11
PVDF-7%AC	0.33 ± 0.01	4.45 ± 0.15
PVDF-9%AC	0.33 ± 0.02	8.56 ± 0.17

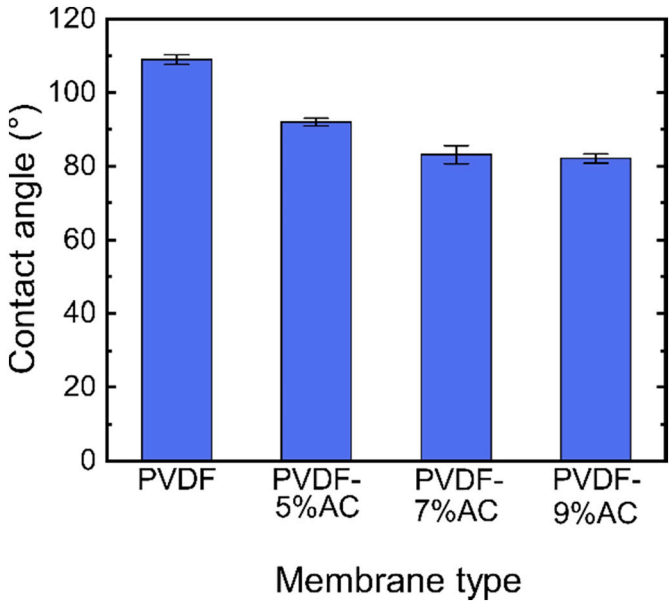

Fig. 4. Contact angle of the pristine and AC-blended membranes.

hydrophilicity, while the 7 % and 9 %AC membranes were distinctly hydrophilic. A hydrophilic membrane is beneficial in this case as it draws salty water into close contact with the hot membrane to facilitate interfacial evaporation. However, an MD membrane needs to be hydrophobic to avoid wetting. We overcame this trade-off by interlaying a commercial hydrophobic PVDF membrane between the PVDF-AC membrane and the air gap. In this case, the PVDF-AC membrane acted as the heating medium, while the commercial PVDF membrane acted as vapor transport medium. This arrangement of two membranes with two different wettabilities helped facilitate water access to the photothermal surface while mitigating the poor salt rejection issue due to PVDF-AC membrane wetting. As a future study, it is possible to eliminate the need for the secondary hydrophobic membrane by controlling the properties (pore size, surface CA, AC content, and pore tortuosity) of the PVDF-AC membrane to have high enough hydrophilicity to facilitate good feed contact but not too high and not too large pore size so that good salt rejection can be maintained.

Fig. 5a and b show the mean pore diameter and porosity, respectively, of pristine and AC-blended PVDF membranes. AC blending increased both the membranes' pore size and porosity. For instance, the 9 %AC-blended PVDF membrane showed an 82 % increase in pore size (0.20 µm) compared to the pristine membrane (0.11 µm). The blending of hydrophilic AC particles into the polymer solution increased the exchange rate between the non-solvent (water) and the solvent (DMAc) during phase separation, resulting in increased pore size, an observation which is consistent with other phase inversion membrane investigations [32,33]. The porosity of the AC-blended PVDF membranes also increased with AC concentration (Fig. 5b), as a result of increased pore size and pore density. The improved openness of the AC-blended membrane, reflected in its higher pore sizes and porosity, helped improve the contact between the feed solution and the membrane surface (both internal and external), thus enhancing the desired transfer of heat from the photothermal membrane to the feed solution.

The results of AC leaching experiments indicate no detectable changes in the membrane mass before and after the leaching tests for all the AC-blended membranes, as shown in Table 3. This suggests that AC is stable within the PVDF-AC membranes.

3.2. AGMD performance of photothermal PVDF-AC membranes

The ability of a photothermal membrane to effectively absorb solar

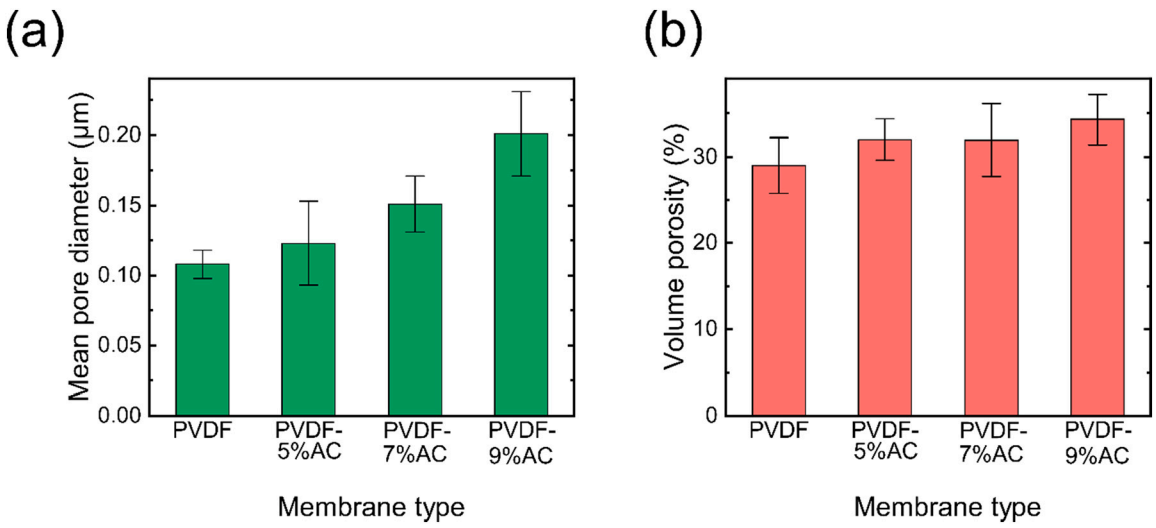

Fig. 5. (a) Mean pore diameter and (b) volume porosity of pristine and PVDF-AC membranes.

Table 3
AC leaching results of the PVDF-AC membranes.

Membrane	Wet weight (mg)	Dry weight (mg)	Leaching (%)
PVDF-5%AC	49	49	0.0
PVDF-7%AC	62	62	0.0
PVDF-9%AC	35	35	0.0

radiation in the broad spectrum and transform it into heat determines its MD efficiency. Fig. 6a depicts the solar absorption spectrum of pristine and AC-blended polymer membranes in the region of 400–1400 nm. Because a considerable percentage of the incident light was reflected from the opaque and white pristine PVDF membrane surface, this membrane displayed minimal light absorption across the entire wavelength range. On the other hand, all PVDF-AC membranes exhibited a substantially higher solar absorbance due to the broadband absorbance and blackbody nature of the embedded AC particles. The results show that the AC can render the PVDF membranes as solar absorbing even at the smallest tested loading (5 %).

The surface temperature of dry pristine and PVDF-AC membranes, when illuminated with solar irradiation at 1 kW m^{-2} power density, was measured using a thermocouple and is presented in Fig. 6b. The surface temperature of the pristine PVDF membrane rose from 23 to 45.6 °C within 11 min of irradiation, then reached a plateau. In contrast, within 11 min of irradiation as well, the surface temperature of the membranes blended with 5, 7, and 9 %AC increased to 78.4, 82.7, and 84.8 °C, respectively. This increase in PVDF-AC temperature, almost double that of pristine membrane, confirms the photothermal properties of the PVDF-AC membranes. The difference between a liquid feed's output and inlet temperature was also measured, with the membranes illuminated with solar radiation in the MD cell (Fig. 6c). The temperature difference for pristine PVDF was about ~1.83 °C, while it was ~2.2, 2.6, and 3.4 °C for 5, 7, and 9%AC membranes, respectively. In the case of feed flow, there is heat loss, via conduction, from the membrane to the feedwater and through the membrane. Unlike conventional MD, in the case of the photothermal membrane, our objective is not to heat the feed as it flows outside the MD cell but to keep the feed heated locally at the membrane surface, where it is most beneficial in generating MD flux. When the feed velocity is low, the feed water on the membrane surface gets enough time to get heated locally and create a significant vapor pressure difference across the membrane. At a high feed flow rate, on the other hand, a higher heat transfer away from the membrane surface will be facilitated, resulting in a lower driving force. Therefore, a low feed flow rate is recommended in the case of PVDF-AC. This is the opposite of conventional MD systems, where an increased feed flow rate usually results in increased permeate flux due to boundary layer suppression [34]. Moreover, because scattering and refraction of solar energy can lower the system's photothermal efficiency, the depth of water layer in the feed channel is another crucial parameter in controlling the amount of solar energy absorbed by the photothermal membranes [35,36].

The photothermal property of the PVDF-AC membranes led to an increased vapor pressure of the feed side during AGMD operation; consequently, the permeate flux also increased significantly (Fig. 7a, b). For instance, the AGMD flux for PVDF-9%AC (0.32 kg.m^{-2}.h^{-1}) was 16-fold that of pristine membrane (0.02 kg.m^{-2}.h^{-1}). These results demonstrate a clear positive correlation between the presence and amount of AC particles within the membrane on one side and the membrane flux on the other. It is important to keep in mind here that while these flux values are much lower than those typically reported for MD systems with active external heating (ca. 3–15 kg.m^{-2}.h^{-1} for most systems [37]), it is important to bear in mind that they were obtained by merely exposing the membrane to solar radiation without an additional system for solar energy harvesting (e.g., solar heater). Another experiment was conducted using PVDF-9%AC without solar irradiation (Fig. 7a, b). The results indicate that PVDF-9%AC, when tested in AGMD under the absence of solar radiation, yielded a permeate flux far below that of the same membrane under solar illumination and much closer to the flux of pristine PVDF. This is evidence that the flux enhancement observed with PVDF-AC membranes is not due to properties other than the photothermal capabilities of AC particles.

The AGMD system performance can be analyzed by determining the membrane distillation coefficient, B. As B is independent of flow conditions and only depends on the membrane's intrinsic properties, it is useful in comparing the MD performance of different membranes. However, as varying the membrane thickness can influence the B value, in the present study, B was divided by the membrane thickness, δ, to get the normalized MD coefficient, B/δ. As shown in Fig. 7c, PVDF-9%AC showed a B/δ value of 18.8×10^{-5} kg s^{-1} m^{-3} Pa^{-1}, 21 times higher than pristine membrane (0.89×10^{-5} kg s^{-1} m^{-3} Pa^{-1}). The MD coefficient has a significant impact on the permeate flux, and this improved B/δ certainly reflects increased mass transfer across the membrane. It is also worth mentioning that localized heating on the surface of the membrane minimizes temperature polarization, hence also contributing to the improved permeate flux [38].

The salt rejection (SR) results shown in Fig. 7d, indicate that all PVDF-AC membranes showed excellent SR, ranging from 97 % for PVDF-5%AC to 99.9 % for PVDF-9%AC. While a slight increase in SR is noticed with the increase in AC loading, it must be remembered that the

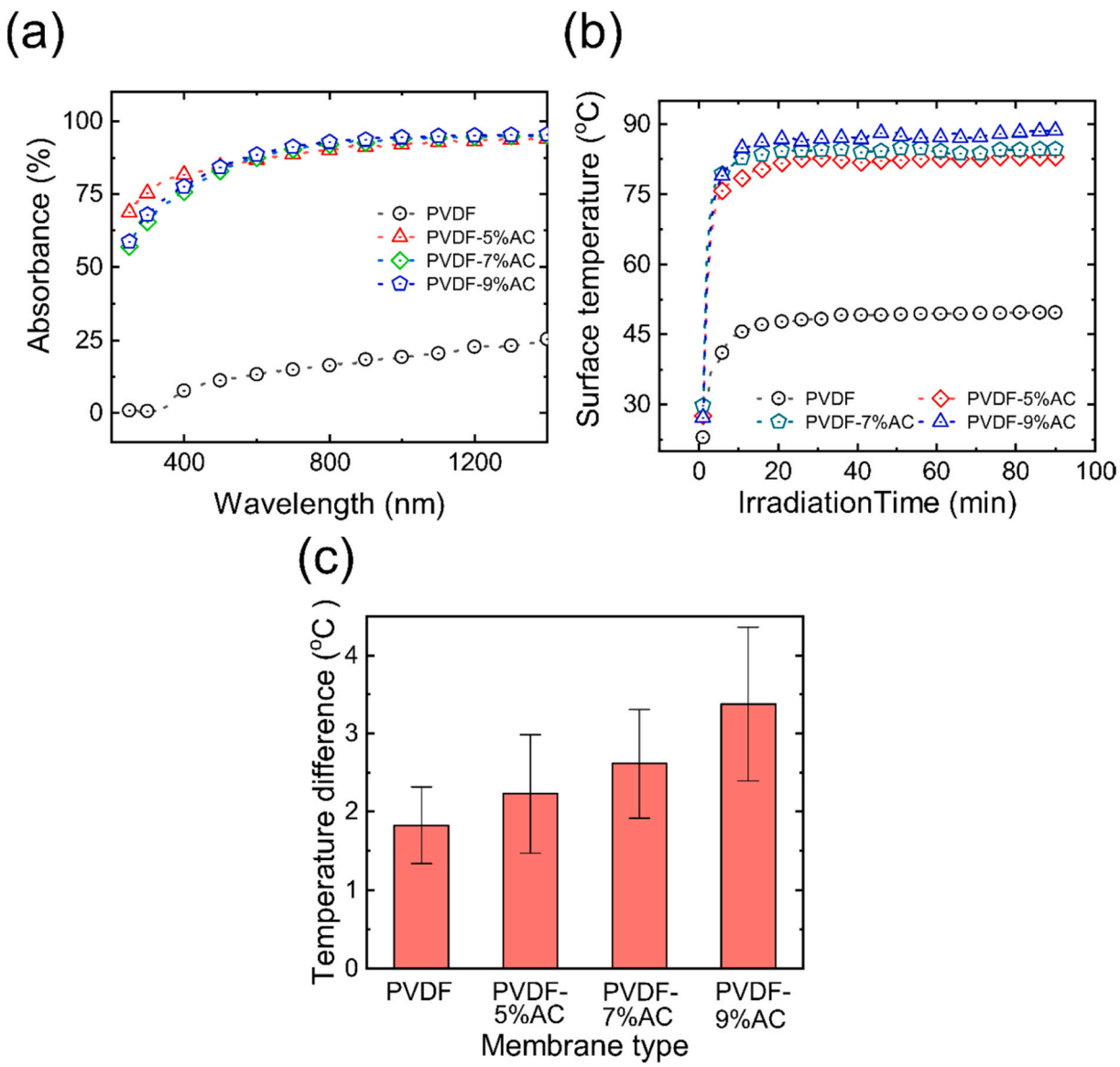

Fig. 6. (a) Solar absorbance of the pristine (PVDF) and AC-blended membranes, (b) Surface temperature of dry membrane under solar irradiation, and (c) temperature difference (feed outlet temperature – feed inlet temperature).

PVDF-AC membranes are hydrophilic and are not the main reason behind the SR, but the inlay commercial membrane is. So, the differences in SR, in this case are probably of no significance. Table 4 summarizes various parameters such as membrane configuration, membrane material, feed and permeate temperatures, flux, number of suns, and energy efficiency of our study with other previously reported studies. Photothermal MD membrane employing antimony doped tin oxide (ATO) nanomaterials, operated in VMD showed the highest maximum flux of 27 $kg.m^{-2}.h^{-1}$. However, a better comparison would be with a membrane containing carbon-based materials. As reported in this study, PVDF/AC membranes operated in AGMD configuration exhibited a flux of 0.31 $kg.m^{-2}.h^{-1}$, whereas PVDF membrane incorporated with carbon black and PVA operated in DCMD configurations exhibited a flux of 0.22 $kg.m^{-2}.h^{-1}$. Thus, the AC-based membrane used in the present study showed better flux than the carbon-black and PVA-based membrane reported earlier. Nevertheless, it is to be noted that comparing the photothermal efficiencies of various membranes operated under different experimental conditions is inaccurate. For instance, some are operated under simulated solar radiation, some with devices to increase the solar radiation intensity on the membrane surface, and others with the actual sun. Therefore, testing the same membrane in different MD configurations or different types of membranes in the same MD system will reveal more insights into significant parameters affecting the photothermal MD performance.

Based on the flux results, the GOR of the system was calculated to assess the thermal efficiency of our best AGMD system using PVDF-9% AC, as shown in Fig. 8a. The GOR using PVDF-9 %AC membrane was 0.29, which stands at 30 % of the maximum theoretical GOR (1.0) of thermal desalination systems without heat recycle. To put this value in context, our GOR value was also compared to other GOR values obtained for three other state-of-the-art photothermal PVDG membranes, also used in AGMD systems, as shown in Fig. 8a. The GOR for PVDF-9%AC was found to be very comparable to a blackbody membrane of PVDF with nitrocellulose and a plasmonic membrane of PVDF and TiN/PVA [16]. Finally, the photothermal efficiency of the PVDF-AC membranes was calculated and is presented in Fig. 8b. As expected, the photothermal efficiency increased with the concentration of AC particles within the PVDF membrane, with PVDF-9%AC exhibiting the maximum efficiency of ~17.64 %, compared to only 1.36 % for the pristine PVDF membrane. This is on par with other photothermal membranes [18].

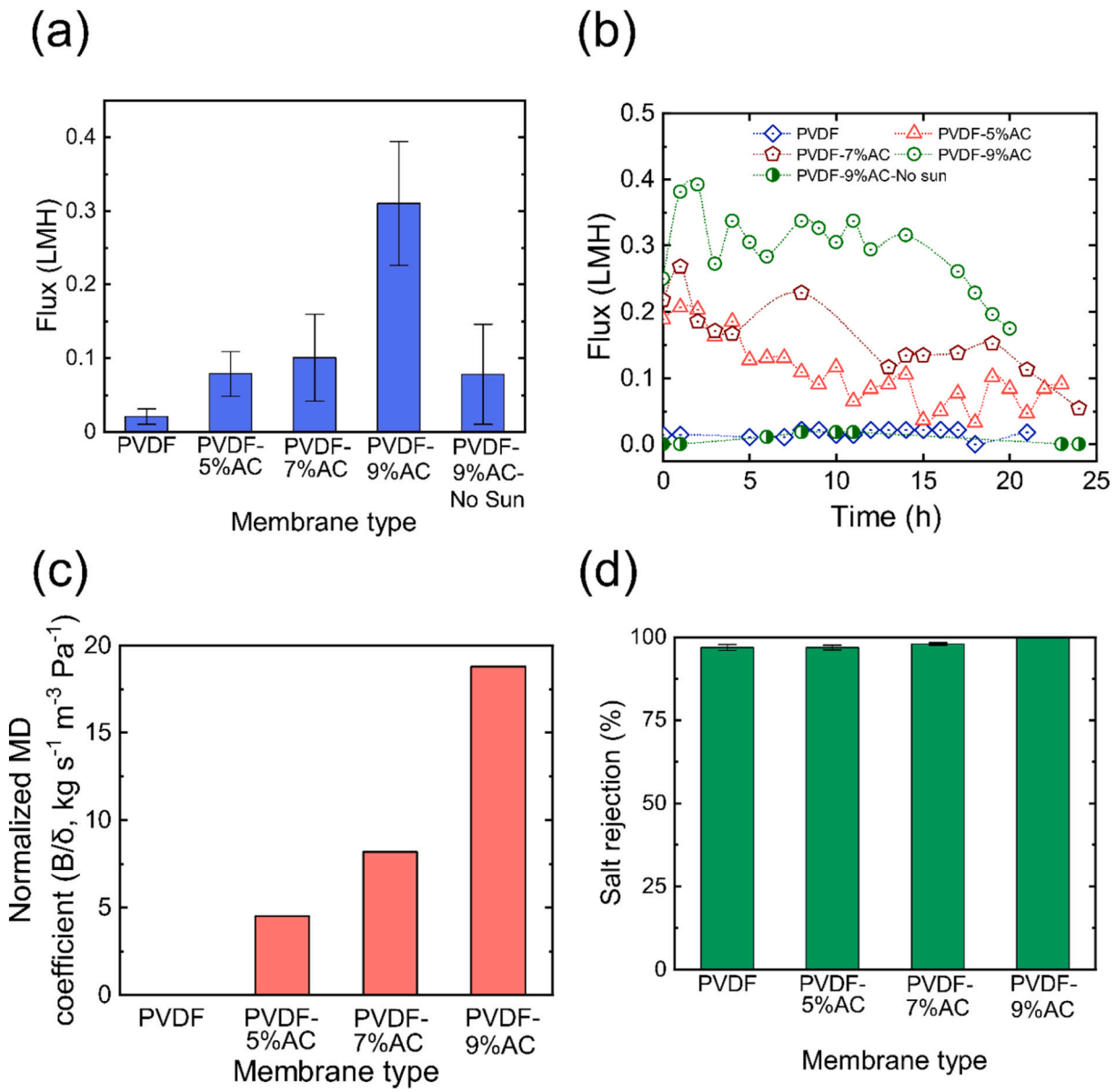

Fig. 7. (a) Average flux, (b) flux over long durations, (c) normalized MD coefficients, and (d) salt rejection for the pristine and PVDF-AC membranes.

Table 4
Comparison of the performance of different materials employed as membranes for solar membrane distillation devices.

MD configuration	Membrane material	Feed temp hot (°C)	Distillate temp cold (°C)	Highest flux (kg.m^{-2}.h^{-1})	Number of suns	Efficiency	Reference
DCMD	PVDF + CB NP + PVA	20	20	5.38	25	20 %	[39]
				0.22	1		
DCMD	PVDF + SiO2/Au	35	20	1.5	1	74.6 %	[40]
VMD	PVDF + Ag NPs	30	20	25	–	20 %	[41]
DCMD	PDA + PVDF	20	20	0.49	1	–	[15]
AGMD	PVDF + nitrocellulose	72	30	0.38	–	20 %	[43]
DCMD	PVDF-HFP + Fe_3O_4	25	20	0.97	1	53 %	[13]
AGMD	PVDF + TiN/PVA	58.73	20	0.94	1	65.8 %	[16]
VMD	PVDF/ATO	70	–	27	–	–	[11]
AGMD	PVDF/AC	23	10	0.31	1	17.63 %	This study

4. Conclusion

A novel PVDF-based photothermal membrane was prepared via phase inversion, in which AC particles were blended at different concentrations (5, 7, and 9 %) without a noticeable agglomeration. The fabricated membranes were characterized, and their performance was evaluated in a photothermal AGMD setup under 1 kW/m^2 simulated solar radiation. SEM images showed that the AC particles were smoothly blended within the PVDF polymer matrix, and the leaching tests confirmed that the AC particles were stable. Increasing the AC concentration in the membrane enhanced the solar absorbance, pore size, and porosity. PVDF membrane blended with 9 %AC demonstrated the

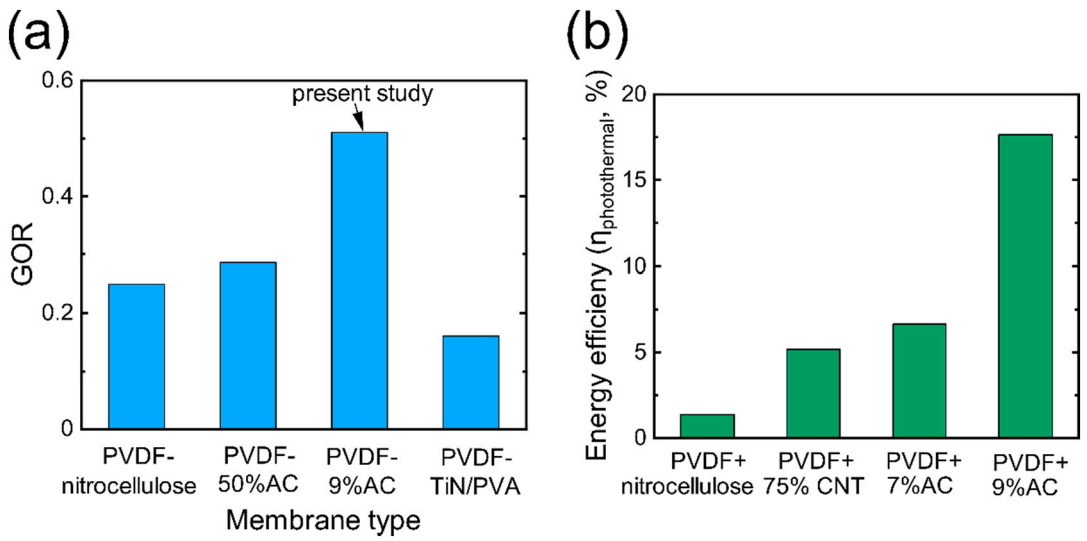

Fig. 8. (a) Comparison of GOR for PVDF-9%AC membrane to a reported blackbody membrane (PVDF + nitrocellulose) and plasmonic membrane (PVDF + TiN/PVA). (b) Comparison of energy efficiency PVDF-9%AC membrane to other reported membranes.

highest average AGMD permeate water flux of 0.31 $kg.m^{-2}.h^{-1}$, with a GOR of 0.29 and a photothermal efficiency of 17.64 %, whereas the pristine PVDF membrane exhibited a flux of only 0.02 $kg.m^{-2}.h^{-1}$. All AC-blended PVDF membranes showed excellent salt rejection, ranging from 97 % for PVDF-5%AC to 99.9 % for PVDF-9%AC. Lastly, the AGMD performance of the fabricated membranes was compared by estimating their normalized MD coefficients (B/δ). PVDF-9%AC exhibited a B/δ value of 18.8×10^{-5} kg s^{-1} m^{-3} Pa^{-1}, as opposed to 0.89×10^{-5} kg s^{-1} m^{-3} Pa^{-1} for the pristine counterpart. The performance of the photothermal AGMD is affected by several operating factors, including feed channel depth and the flow rate of feedwater, which need to be investigated further to improve the photothermal performance of the membranes. Likewise, more research is needed on optimizing the AGMD module designs to amplify the incoming solar radiation and facilitate sufficient heat recovery, which will enable the wide-scale practical applications of photothermal membrane distillation processes.

CRediT authorship contribution statement

Maryam Alqaydi: Conceptualization, Methodology, Data curation, Writing – Original draft preparation, Visualization.

Musthafa O. Mavukkandy: Investigation, Data curation, Reviewing and Editing, Validation.

Ibrahim Mustafa: Methodology, Data acquisition.

Aaesha Alnuaimi: Reviewing and Editing.

Hassan A. Arafat: Conceptualization, Methodology, Reviewing and Editing, Supervision, Validation.

Faisal Almarzooqi: Conceptualization, Methodology, Reviewing and Editing, Supervision, Validation.

Declaration of competing interest

The authors declare that they have no known competing financial interests or personal relationships that could have appeared to influence the work reported in this paper.

Data availability

Data will be made available on request.

Acknowledgement

The authors are grateful to Ms. Alaa Shaheen for her assistance in the solar MD experiments and illustration of the AGMD setup, and Ms. Fu Jing from Prof. Kin Liao's team at Khalifa University for her help in membrane characterizing. This study was funded by Khalifa University (award No. CIRA 2019-004) and the Center for Membrane and Advanced Water Technology (CMAT) at Khalifa University (award No. RC2-2018-009).

References

[1] UNESCO, The United Nations World Water Development Report 2018, Nature-Based Solutions for Water, 2018.
[2] Technavio, Global Desalination Market 2018–2022, 2018.
[3] P. Zhang, J. Li, L. Lv, Y. Zhao, L. Qu, Vertically aligned graphene sheets membrane for highly efficient solar thermal generation of clean water, ACS Nano 11 (2017) 5087–5093, https://doi.org/10.1021/acsnano.7b01965.
[4] V.G. Gude, N. Nirmalakhandan, S. Deng, Desalination using solar energy: towards sustainability, Energy 36 (2011) 78–85, https://doi.org/10.1016/j.energy.2010.11.008.
[5] S.A. Kalogirou, Seawater desalination using renewable energy sources, Prog. Energy Combust. Sci. 31 (2005) 242–281, https://doi.org/10.1016/j.pecs.2005.03.001.
[6] F.A. Banat, J. Simandl, Desalination by membrane distillation: a parametric study 6395 (2008), https://doi.org/10.1080/01496399808544764.
[7] M.R. Qtaishat, F. Banat, Desalination by solar powered membrane distillation systems, Desalination 308 (2013) 186–197, https://doi.org/10.1016/J.DESAL.2012.01.021.
[8] J.H.L.V. E.K. Summers, Experimental study of thermal performance in air gap membrane distillation systems, including the direct solar heating of membranes, DES 330 (2013) 100–111, https://doi.org/10.1016/j.desal.2013.09.023.
[9] F. Zhao, Y. Guo, X. Zhou, W. Shi, G. Yu, Materials for solar-powered water evaporation, Nat. Rev. Mater. 5 (2020), https://doi.org/10.1038/s41578-020-0182-4.
[10] P.D. Dongare, A. Alabastri, S. Pedersen, K.R. Zodrow, N.J. Hogan, O. Neumann, J. Wud, T. Wang, A. Deshmukh, M. Elimelech, Q. Li, P. Nordlander, N.J. Halas, Nanophotonics-enabled solar membrane distillation for off-grid water purification, Proc. Natl. Acad. Sci. U. S. A. 114 (2017) 6936–6941, https://doi.org/10.1073/pnas.1701835114.
[11] Q. Huang, S. Gao, Y. Huang, M. Zhang, C. Xiao, Study on photothermal PVDF/ATO nanofiber membrane and its membrane distillation performance, J. Membr. Sci. 582 (2019) 203–210, https://doi.org/10.1016/j.memsci.2019.04.019.
[12] Q.L.Jinjian Wua, Katherine R. Zodrowa, Peter B. Szemraja, Photothermal nanocomposite membranes for direct solar membrane distillation, 2017, https://doi.org/10.1039/C7TA04555G. Published.
[13] W. Li, Y. Chen, L. Yao, X. Ren, Y. Li, L. Deng, Fe3O4/PVDF-HFP photothermal membrane with in-situ heating for sustainable, stable and efficient pilot-scale solar-driven membrane distillation, Desalination 478 (2020), 114288, https://doi.org/10.1016/j.desal.2019.114288.
[14] A. Politano, P. Argurio, G. Di Profio, V. Sanna, A. Cupolillo, S. Chakraborty, H. A. Arafat, E. Curcio, in: Photothermal membrane distillation for seawater desalination, 2017, pp. 1–6, https://doi.org/10.1002/adma.201603504.
[15] X. Wu, Q. Jiang, D. Ghim, S. Singamaneni, Y.S. Jun, Localized heating with a photothermal polydopamine coating facilitates a novel membrane distillation

process, J. Mater. Chem. A 6 (2018) 18799–18807, https://doi.org/10.1039/c8ta05738a.
[16] Y. Zhang, K. Li, L. Liu, K. Wang, J. Xiang, D. Hou, J. Wang, Titanium nitride nanoparticle embedded membrane for photothermal membrane distillation, Chemosphere 256 (2020), 127053, https://doi.org/10.1016/j.chemosphere.2020.127053.
[17] L. Zhao, C. Wu, X. Lu, D. Ng, Y. Bach, Z. Xie, in: Activated carbon enhanced hydrophobic/hydrophilic dual-layer nanofiber composite membranes for high-performance direct contact membrane distillation 446, 2018, pp. 59–69, https://doi.org/10.1016/j.desal.2018.09.002.
[18] A. Shaheen, S. AlBadi, B. Zhuman, H. Taher, F. Banat, F. AlMarzooqi, Photothermal air gap membrane distillation for the removal of heavy metal ions from wastewater, Chem. Eng. J. 431 (2022), 133909, https://doi.org/10.1016/J.CEJ.2021.133909.
[19] L. Marbelia, M.R. Bilad, I.F.J. Vankelecom, Gradual PVP leaching from PVDF/PVP blend membranes and its effects on membrane fouling in membrane bioreactors, Sep. Purif. Technol. 213 (2019) 276–282, https://doi.org/10.1016/J.SEPPUR.2018.12.045.
[20] R. Thomas, E. Guillen-Burrieza, H.A. Arafat, Pore structure control of PVDF membranes using a 2-stage coagulation bath phase inversion process for application in membrane distillation (MD), J. Membr. Sci. 452 (2014) 470–480, https://doi.org/10.1016/J.MEMSCI.2013.11.036.
[21] E. Guillen-Burrieza, R. Thomas, B. Mansoor, D. Johnson, N. Hilal, H. Arafat, Effect of dry-out on the fouling of PVDF and PTFE membranes under conditions simulating intermittent seawater membrane distillation (SWMD), J. Membr. Sci. 438 (2013) 126–139, https://doi.org/10.1016/J.MEMSCI.2013.03.014.
[22] S. Mansour, A. Giwa, S.W. Hasan, Novel graphene nanoplatelets-coated polyethylene membrane for the treatment of reject brine by pilot-scale direct contact membrane distillation: an optimization study, Desalination 441 (2018) 9–20, https://doi.org/10.1016/j.desal.2018.04.026.
[23] K. Huang, Q. Zhang, F. Yang, D. He, Ultraviolet photoconductance of a single hexagonal Wo3 nanowire, Nano Res. 3 (2010) 281–287, https://doi.org/10.1007/s12274-010-1031-3.
[24] H. Geng, H. Wu, P. Li, Q. He, Study on a new air-gap membrane distillation module for desalination, Desalination 334 (2014) 29–38, https://doi.org/10.1016/J.DESAL.2013.11.037.
[25] M.A.-J.M. Smith, Hendrick C. Van Ness, Introduction to Chemical Engineering Thermodynamics, 7th ed., McGraw-Hill Education, Europe, 2005.
[26] T.H. Bae, T.M. Tak, Effect of TiO2 nanoparticles on fouling mitigation of ultrafiltration membranes for activated sludge filtration, J. Membr. Sci. 249 (2005) 1–8, https://doi.org/10.1016/J.MEMSCI.2004.09.008.
[27] S. Zinadini, A.A. Zinatizadeh, M. Rahimi, V. Vatanpour, H. Zangeneh, Preparation of a novel antifouling mixed matrix PES membrane by embedding graphene oxide nanoplates, J. Membr. Sci. 453 (2014) 292–301, https://doi.org/10.1016/J.MEMSCI.2013.10.070.
[28] J. Ren, J. Zhou, M. Deng, Morphology transition of asymmetric polyetherimide flat sheet membranes with different thickness by wet phase-inversion process, Sep. Purif. Technol. 74 (2010) 119–129, https://doi.org/10.1016/J.SEPPUR.2010.05.014.
[29] M.O. Mavukkandy, Q. Zaib, H.A. Arafat, CNT/PVP blend PVDF membranes for the removal of organic pollutants from simulated treated wastewater effluent, J. Environ. Chem. Eng. 6 (2018) 6733–6740, https://doi.org/10.1016/J.JECE.2018.10.029.
[30] Y. Agari, T. Uno, Thermal conductivity of polymer filled with carbon materials: effect of conductive particle chains on thermal conductivity, J. Appl. Polym. Sci. 30 (1985) 2225–2235, https://doi.org/10.1002/app.1985.070300534.
[31] X. Song, H. Liu, L. Cheng, Y. Qu, Surface modification of coconut-based activated carbon by liquid-phase oxidation and its effects on lead ion adsorption, Desalination 255 (2010) 78–83, https://doi.org/10.1016/J.DESAL.2010.01.011.
[32] B.S. Lalia, V. Kochkodan, R. Hashaikeh, N. Hilal, A review on membrane fabrication: structure, properties and performance relationship, Desalination 326 (2013) 77–95, https://doi.org/10.1016/j.desal.2013.06.016.
[33] X.M. Tan, D. Rodrigue, A review on porous polymeric membrane preparation. Part II: production techniques with polyethylene, polydimethylsiloxane, polypropylene, polyimide, and polytetrafluoroethylene, Polymers (Basel) 11 (2019), https://doi.org/10.3390/polym11081310.
[34] K. Sardari, P. Fyfe, S. Ranil Wickramasinghe, Integrated electrocoagulation – forward osmosis – membrane distillation for sustainable water recovery from hydraulic fracturing produced water, J. Membr. Sci. 574 (2019) 325–337, https://doi.org/10.1016/J.MEMSCI.2018.12.075.
[35] M. Gao, C.K. Peh, F.L. Meng, G.W. Ho, Photothermal membrane distillation toward solar water production, Small Methods 5 (2021), 2001200, https://doi.org/10.1002/SMTD.202001200.
[36] R. Tripathi, G.N. Tiwari, Effect of water depth on internal heat and mass transfer for active solar distillation, Desalination 173 (2005) 187–200, https://doi.org/10.1016/J.DESAL.2004.08.032.
[37] M. Qasim, I.U. Samad, N.A. Darwish, N. Hilal, Comprehensive review of membrane design and synthesis for membrane distillation, Desalination 518 (2021), 115168, https://doi.org/10.1016/J.DESAL.2021.115168.
[38] A. Politano, G. di Profio, E. Fontananova, V. Sanna, A. Cupolillo, E. Curcio, Overcoming temperature polarization in membrane distillation by thermoplasmonic effects activated by Ag nanofillers in polymeric membranes, Desalination 451 (2019) 192–199, https://doi.org/10.1016/J.DESAL.2018.03.006.
[39] P.D. Dongare, A. Alabastri, S. Pedersen, K.R. Zodrow, N.J. Hogan, O. Neumann, J. Wud, T. Wang, A. Deshmukh, M. Elimelech, Q. Li, P. Nordlander, N.J. Halas, Nanophotonics-enabled solar membrane distillation for off-grid water purification, Proc. Natl. Acad. Sci. U. S. A. 114 (2017) 6936–6941, https://doi.org/10.1073/PNAS.1701835114/SUPPL_FILE/PNAS.201701835SI.PDF.
[40] J. Wu, K.R. Zodrow, P.B. Szemraj, Q. Li, Photothermal nanocomposite membranes for direct solar membrane distillation, J. Mater. Chem. A 5 (2017) 23712–23719, https://doi.org/10.1039/C7TA04555G.
[41] A. Politano, P. Argurio, G. di Profio, V. Sanna, A. Cupolillo, S. Chakraborty, H. A. Arafat, E. Curcio, Photothermal membrane distillation for seawater desalination, Adv. Mater. 29 (2017), 1603504, https://doi.org/10.1002/ADMA.201603504.
[43] E.K. Summers, J.H. Lienhard, Experimental study of thermal performance in air gap membrane distillation systems, including the direct solar heating of membranes, Desalination 330 (2013) 100–111, https://doi.org/10.1016/J.DESAL.2013.09.023.